

Distance-Dependent Fluorescence Quenching of *N*-Acetyl-L-Tryptophanamide by Acrylamide

Bogumil Zelent,¹ Józef Kuśba,¹ Ignacy Gryczynski,¹ Michael L. Johnson,² and Joseph R. Lakowicz¹

Received October 18, 1993

We examined the time-dependent intensity decays of *N*-acetyl-L-tryptophanamide (NATA) when collisionally quenched by acrylamide in propylene glycol over a range of temperatures. The intensity decays of NATA became increasingly heterogeneous in the presence of acrylamide. The NATA intensity decays were not consistent with the Collins–Kimball radiation boundary condition (RBC) model for quenching. The steady-state Stern–Volmer plots show significant upward curvature, and quenching of NATA by acrylamide was observed even in vitrified propylene glycol, where translational diffusion cannot occur during the lifetime of the excited state. These frequency-domain and steady-state data indicate a through-space quenching interaction between NATA and acrylamide, and the results are consistent with a rate constant for quenching that depends exponentially on the fluorophore–quencher separation distance. The exponential distance-dependent rate of quenching also explains the upward curvature of the Stern–Volmer plot, and the steady-state data aid in determining the interaction distance between NATA and acrylamide. These results suggest that the distance-dependent quenching rates need to be considered in the interpretation of acrylamide quenching of proteins.

KEY WORDS: *N*-Acetyl-L-tryptophanamide; tryptophan fluorescence intensity decay; frequency-domain fluorometry; fluorescence spectroscopy; distance-dependent quenching.

INTRODUCTION

The phenomenon of collisional quenching of fluorescence has been a long-standing interest in physical chemistry and biochemistry. The applications of these studies include investigations of structure and dynamics of proteins [1–5] and membranes [6,7]. Collisional quenching requires contact between the fluorophores and the quencher during the lifetime of the excited state. Studies of quenching can yield information about diffusive motions in solution, the accessibility of fluoro-

phores in macromolecules to externally added quenchers, and the diffusion of quenchers within proteins and macromolecules. It is known that single-exponential decays of fluorophores in the presence of quenching become nonexponential, due to transient effects [8–11] that occur immediately following excitation. The origin of the transient effects in collisional quenching of fluorescence is the rapid decay of closely spaced fluorophore–quencher pairs, followed by slower diffusion-limited quenching of the remaining fluorophores. We have emphasized that these effects can be readily detected by using frequency-domain fluorometry [10–13]. An important feature of the analysis is the ability independently to recover diffusion coefficients, interaction radii, and specific rate constants for quenching. The diffusion coefficients are

¹ Center for Fluorescence Spectroscopy, Department of Biological Chemistry, University of Maryland at Baltimore, School of Medicine, 108 North Greene Street, Baltimore, Maryland 21201.

² Department of Pharmacology, University of Virginia, Box 448, Jordan Hall, Room 561, Charlottesville, Virginia 22908.

of particular interest for fluorophores in proteins and membranes.

Collisional quenching of fluorescence usually is interpreted based on the theory of Smoluchowski [8,14,15]. The theory assumes that the fluorophore is immediately quenched upon contact with quencher and instantaneously returns to the ground state. This model predicts a transient term in the diffusion equation that results in nonexponential decays of fluorescence intensity. The Smoluchowski model [15] developed by Collins and Kimball [16] assumes a specific rate constant for quenching (κ) at a given fluorophore–quencher distance. This model, named the radiation boundary condition (RBC), becomes equivalent to Smoluchowski's model when the value of κ approaches infinity. The frequency-domain measurements [10,11,17] and recent results for the quenching of POPOP [18] and anthracenes [19] indicated that the phenomenon of collisional quenching is not completely described by the RBC model but requires a distance-dependent rate constant for quenching, referred to as the DDQ model. These two models for collisional quenching of fluorescence are presented in Scheme I. The RBC model for the rate of quenching $k(r)$ assumes a value of $\kappa\delta(r - a)$ at the encounter distance a , which is the distance of the fluorophore–quencher closest approach, and the quenching rate is zero elsewhere. In this model, no specific form of the intermolecular interaction

is assumed. The DDQ model assumes for the bimolecular quenching rate has the following form:

$$k(r) = k_a \exp\left(-\frac{r-a}{r_e}\right) \quad (1)$$

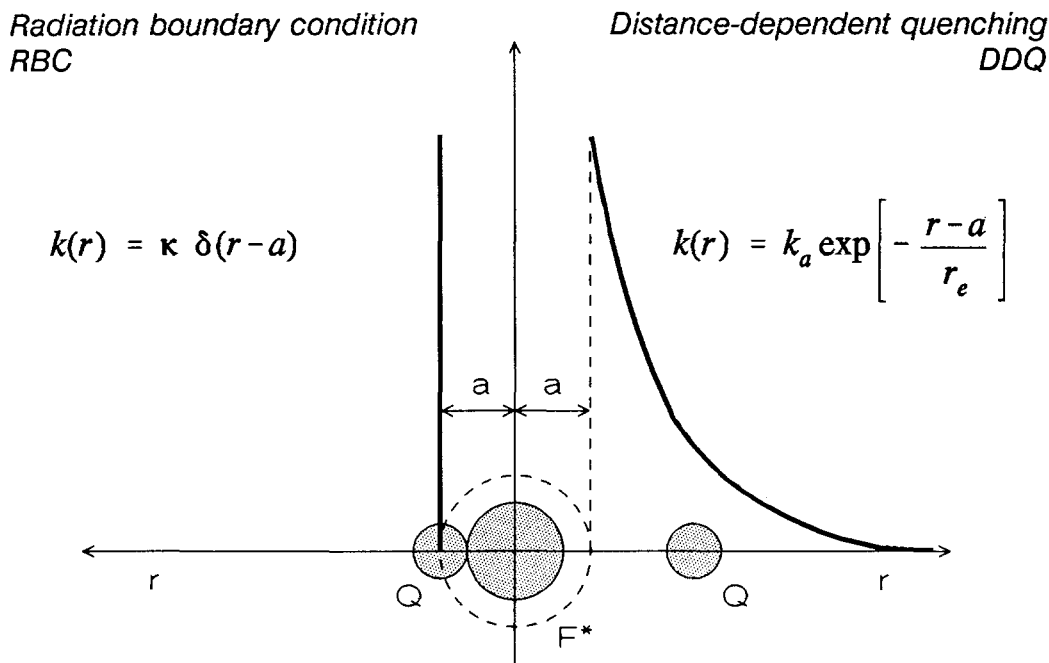
where r_e is the characteristic transfer distance, a is the distance of closest approach, and k_a is the value of quenching rate at $r = a$. Equation (1) is appropriate electron transfer and electron exchange interactions as proposed by Dexter [20].

In the present report using gigahertz frequency-domain fluorometry [21,22] and global analysis, we extend detailed studies on the time-dependent intensity decays of *N*-acetyl-L-tryptophanamide (NATA) when collisionally quenched by acrylamide in propylene glycol at 20, –20 and –60°C. The structure of NATA is representative of tryptophan residues in proteins. Acrylamide is widely used as a polar and neutral quencher of protein fluorescence [23].

THEORY

Mono- and Multiexponential Intensity Decays

The fluorophore intensity decay $[I(t)]$ in the absence of quenchers for a single exponential is given by



Scheme I. Comparison of the radiation boundary condition and distance-dependent quenching models for collisional quenching of fluorescence.

$$I(t) = I^0 \exp(-t/\tau_0) \quad (2)$$

where τ_0 is the decay time of the fluorophore. A multiexponential intensity decay is described by

$$I(t) = \sum_i \alpha_i \exp(-t/\tau_i) \quad (3)$$

where τ_i are the individual decay times and α_i are the associated preexponential factors. The fractional contribution of each decay time component to the steady-state intensity is

$$f_i = \frac{\alpha_i \tau_i}{\sum_j \alpha_j \tau_j} \quad (4)$$

where $\sum f_i = 1$, $\sum \alpha_i = 1$, and the mean decay time is expressed as

$$\bar{\tau} = \sum_i f_i \tau_i \quad (5)$$

Intensity Decays in the Presence of Quenching

In the presence of quenching the time-dependent fluorophore intensity decay can be described by

$$I(t) = I_0 \exp \left[-\frac{t}{\tau_0} - C_q^0 \int_0^t k(t') dt' \right] \quad (6)$$

where τ_0 is the unquenched fluorophore lifetime, C_q^0 is the bulk concentration of the quencher, and $k(t)$ denotes the averaged time-dependent second-order rate of quenching. The rate $k(t)$ can be expressed as

$$k(t) = \frac{4\pi}{C_q^0} \int_a^\infty r^2 k(r) C_q(r, t) dr \quad (7)$$

where $C_q(r, t)$ is the concentration of the quencher molecules at the distance r from the excited fluorophore at time instant t . The rate $k(t)$ may involve two terms: the transient term, which rapidly decays; and the time independent term, which describes the kinetics of quenching at very long times.

Frequency-Domain Fluorometry

Using the technique of frequency-domain fluorometry [21,22], the parameters describing the intensity decay of the fluorophore emission are the phase (ϕ_ω) and modulation (m_ω) of the emission over a range of modulation frequencies (ω), in $\text{rad} \times \text{s}^{-1}$. The calculated (c) phase and modulation values from the model

intensity decay $I(t)$ at a given frequency are described as

$$\phi_{c\omega} = \arctan(N_\omega/D_\omega) \quad (8)$$

$$m_{c\omega} = \frac{1}{J} (N_\omega^2 + D_\omega^2)^{1/2} \quad (9)$$

where

$$N_\omega = \int_0^\infty I(t) \sin(\omega t) dt \quad (10)$$

$$D_\omega = \int_0^\infty I(t) \cos(\omega t) dt \quad (11)$$

$$J = \int_0^\infty I(t) dt \quad (12)$$

The most probable parameter values and goodness of fit are determined by the minimum value of

$$\chi_R^2 = \frac{1}{\nu} \sum_\omega \left(\frac{\phi_\omega - \phi_{c\omega}}{\delta\phi} \right)^2 + \frac{1}{\nu} \sum_\omega \left(\frac{m_\omega - m_{c\omega}}{\delta m} \right)^2 \quad (13)$$

where ν is the number of degrees of freedom and $\delta\phi$ and δm are the experimental uncertainties. Using the best-fit parameter values we calculate the relative quantum yield of the fluorophore, defined as

$$F/F_0 = \frac{\int_0^\infty I(t) dt}{\int_0^\infty I^0(t) dt} \quad (14)$$

where $I(t)$ and $I^0(t)$ are expressed by Eqs. (6) and (2), respectively.

MATERIALS AND METHODS

Phase and modulation fluorescence measurements were performed using the gigahertz frequency-domain fluorometer described previously in detail [21,22]. The excitation wavelength was 296 nm, from a frequency-doubled R6G dye laser (Coherent, Inc). The modulated excitation was provided by the harmonic content of a laser pulse train with a repetition rate of 3.795 MHz and a pulse width of about 7 ps. The dye laser was pumped with a mode-locked argon ion laser (Coherent, Innova

15). The emitted light was detected using a microchannel plate PMT (Hamamatsu R1564U) with external cross-correlation. All intensity decays were measured using rotation-free polarization conditions (magic-angle polarizer orientation) to avoid the effects of Brownian rotation. The fluorophore emission was selected by a combination of Schott WG-335 and Corning 7-51 filters (Fig. 1). At each modulation frequency we measure the phase and modulation of the sample and the reference, which was PPD in ethanol ($\tau = 1.25, 1.26,$ and 1.27 ns at $20, -20$ and -60°C , respectively) [22]. The background fluorescence and/or scattered light of acrylamide in propylene glycol contribute less than 0.5% to the measured emission. The data were collected using a dedicated Minc11/23 computer and then transferred to a Silicon Graphics IRIS CS/12 computer for analysis. For all analysis the uncertainties ($\delta\phi$ and δm) were taken as 0.2° in the phase angle and 0.005 in the modulation ratio, respectively. Steady-state fluorescence measurements were carried out with an SLM 8000 photon-counting spectrofluorometer equipped with a thermostated cell holder. The emission was detected using a photomultiplier tube, R928 (Hamamatsu). For varying temperatures we used

an Endocal ULT-80 thermostat (Neslab). Absorption spectra were measured on a Perkin-Elmer Lambda 6, UV/VIS spectrophotometer.

N-Acetyl-L-tryptophanamide (NATA) was from Aldrich and acrylamide (>99.9% electrophoresis purity reagent; Lot 32285) was from Bio-Rad. 1,2-Propanediol (propylene glycol; P.A. grade) was from Janssen Chimica. The concentration of NATA in the samples was $\approx 5 \times 10^{-4}$ M and was precisely the same in all samples, while the concentration of acrylamide ranged from 0 to 1.5 M at 20°C . At -20 and -60°C the concentration of acrylamide was calculated based on the measured decreases in the volume of the solution, which were 2.3 and 4.6%, correspondingly, compared to the volume of solution at 20°C . The solutions were not purged to remove dissolved oxygen. The emission spectra of NATA were measured using 1×0.4 -cm cells. The excitation wavelength of 296 nm for acrylamide quenching of NATA was selected to minimize background absorption by the quencher. Steady-state intensity emission of NATA in propylene glycol was corrected for the absorption of acrylamide (A_Q^{296}) at the excitation wavelength. A correction factor, $-\log(A_Q^{296}/2)$, was applied [24].

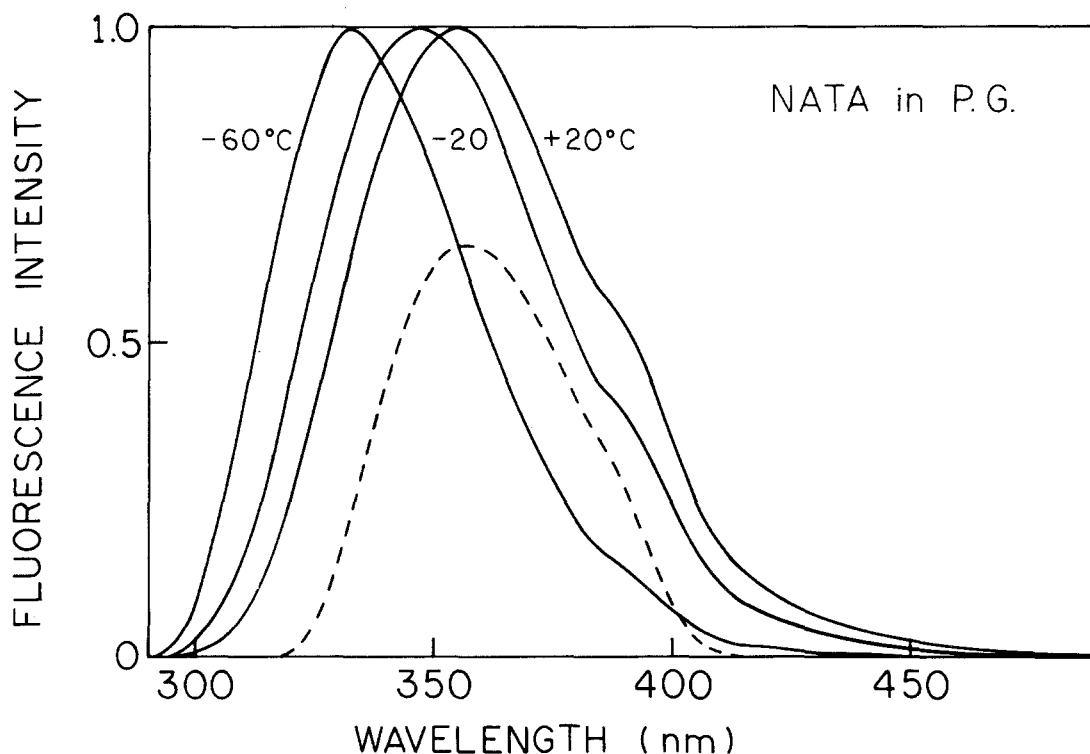


Fig. 1. Fluorescence emission spectra of NATA in propylene glycol. The dashed line shows the emission spectrum of NATA observed through the combination of Schott WG-335 and Corning 7-51 filters used to select the emission for intensity decay measurements.

RESULTS

The emission spectra of NATA in propylene glycol at 20, -20, and -60°C are shown in Fig. 1. At 20°C the maximum of the emission band appears near 355 nm and progressively shifts to higher energy when temperature of the solution decreases. The blue shift of the emission spectrum is due to the solvent viscosity effect which can be explained by the inability of the solvent molecules to reorient during lifetime of the excited state of NATA. For all temperatures the intensity decay of NATA was measured using the emission observed through the combination of filters as also shown in Figure 1.

Figure 2 shows the frequency-response of the fluorescence intensity decays of NATA in propylene glycol in the absence and presence of acrylamide over a range of temperatures. It is clearly shown that at 20 and at -60°C, the experimental data points for NATA (●) can be satisfactorily fitted using monoexponential decays with $\tau = 5.277$ ns ($\chi_R^2 = 1.23$) and $\tau = 5.516$ ns ($\chi_R^2 = 2.15$), respectively. However, at -20°C a monoexponential decay fit ($\tau = 6.711$ ns) is not acceptable to account for experimental points as can be judged by $\chi_R^2 = 23.65$. In fact we need a three-decay time fit, with one negative lifetime component. This is due to spectral relaxation of the emission of NATA at this intermediate temperature. The multiexponential analysis yields $\tau_1 = 8.519$ ns ($\alpha_1 = 0.317$), $\tau_2 = 4.953$ ns ($\alpha_2 = 0.464$), and $\tau_3 = 0.277$ ns ($\alpha_3 = -0.219$) with $\chi_R^2 = 0.45$.

As shown in Fig. 2, the intensity decays of NATA become heterogeneous in the presence of acrylamide (○). The addition of 1.0 M acrylamide results in a decrease in the mean decay times (eq. 5) from 5.277 to 1.755 ns at 20°C, from 6.794 to 4.962 ns at -20°C, and from 5.509 to 4.595 ns at -60°C. This effect is also shown in Fig. 3. When the concentration of acrylamide increases from 0.0 to 1.5, 1.535, or 1.572 M, correspondingly the fluorescence intensity decay of NATA becomes increasingly heterogeneous. This results in progressive shifting of the frequency response to higher frequencies, indicating a progressive decrease in the mean decay time. When NATA is quenched by acrylamide, mono- and two-exponential decays are not acceptable to fit the experimental points. Only three-decay lifetime components account satisfactorily for the data.

Frequency responses of the fluorescence intensity decays of NATA in propylene glycol when quenched by acrylamide were analyzed using two models for collisional quenching of fluorescence. These analyses for the RBC and DDQ models are shown in Tables I and II, respectively. To compare the models, we performed global analyses of the frequency-domain data at 20, -20, and

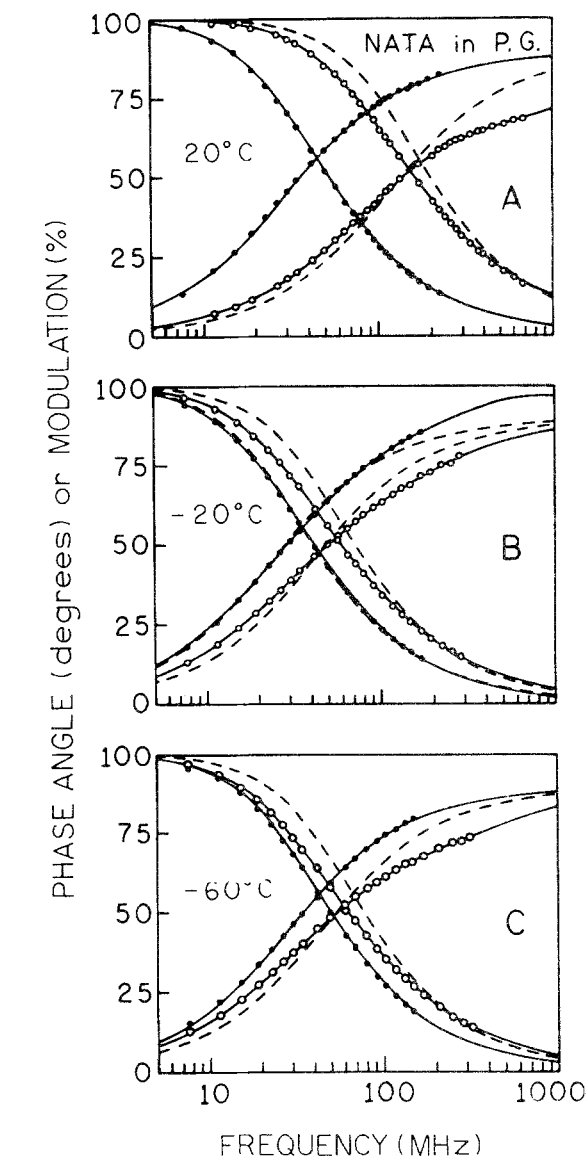


Fig. 2. Frequency-response of the NATA intensity in propylene glycol (A) at 20°C, (B) at -20°C, and (C) at -60°C in the absence (●) and presence (○) of 1 M acrylamide. Solid lines show the best mono- or triple-exponential fit to the data. Dashed lines show the best fit to the data using monoexponential decays.

-60°C. For all concentrations of acrylamide at each temperature, we used the same variable parameters, which are a , D , and κ for the RBC model and a , k_a , r_e , and D for the DDQ model. In these analyses the intensity decay unquenched NATA is held constant at the values indicated by the single- or multiexponential decay laws listed in Tables I and II. Previously [25] we emphasized that for NATA quenched by acrylamide in propylene glycol,

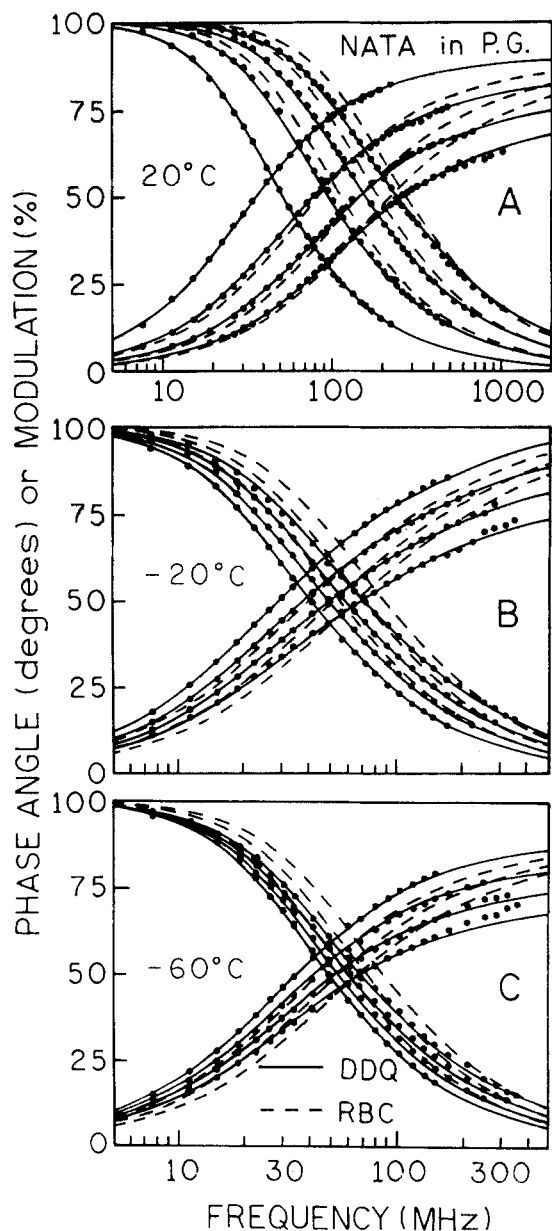


Fig. 3. Frequency-domain intensity decays of NATA in propylene glycol in the presence of increasing (left to right) concentrations of acrylamide: (A) 0, 0.5, 1.0, and 1.5 *M* at 20°C; (B) 0, 0.512, 1.023, and 1.535 *M* at -20°C; and (C) 0, 0.524, 1.048, and 1.572 *M* at -60°C. The solid lines show the best fit to the DDQ model (Table II); and the dashed lines, to the RBC model (Table I).

the most proper distance of the closest approach appears to be $a = 5 \text{ \AA}$.

The best global fits to the data at all acrylamide concentration are shown in Fig. 3. It is clearly shown in

Table I. Global RBC Analysis^a of NATA Quenching by Acrylamide in Propylene Glycol at Different Temperatures

Temp. (°C)	τ_i (ns)	α_i	C_Q (M)	κ (cm/s)	D (cm ² /s)	χ_R^2
20	5.277	1.000	0	∞	7.18×10^{-7}	143.12
			0.500			
			1.000			
			1.500			
-20	8.519	0.317	0	∞	1.25×10^{-7}	193.31
		0.464	0.512			
		-0.219	1.023			
			1.535			
-60	12.432	0.020	0	∞	8.99×10^{-8}	132.86
		0.980	0.524			
			1.048			
			1.572			

^aThe distance of the closest approach a was held constant at 5 \AA during the analysis.

Fig. 3 (dashed lines) that the RBC model cannot account for the intensity decay of NATA quenched by acrylamide at 20, -20, and -60°C. The deviations between the best-fit RBC model and experimental data points are apparent at the higher frequencies. The deviations appear to be due to the presence of a short decay time component in the intensity decays that cannot be accounted for by the RBC model. The RBC model does not predict any quenching in the absence of diffusion and, thus, cannot account for the quenching of NATA seen at -60°C (Fig. 3C and Table I). We also questioned whether the quantum yields predicted from the best RBC-fit intensity decay [Eq. (14)] were consistent with the measured amount of quenching. The measured values of F_0/F are shown in Fig. 4 (●) along with the prediction of the RBC model. Evidently, the RBC model cannot explain the extents of steady-state quenching at 20 and -20°C. At -60°C, and with no diffusion, the RBC model predicts no quenching ($F_0/F = 1$ in Fig. 4C).

In contrast to the RBC model, the DDQ model was found to be consistent with the experimental data in all temperatures. The results of the global analyses from the DDQ model are presented in Table II. The best global fit to the data obtained from the DDQ model is shown by the low values of χ_R^2 (Table II) and by the good agreement between the calculated and the measured frequency-domain decays at 20, -20, and -60°C (Fig. 3). Also, the calculated quantum yields are in excellent agreement with the steady-state (F_0/F) values (Fig. 4). In this analysis we found that values of F_0/F were sen-

Table II. Global DDQ Analysis^a of NATA Quenching by Acrylamide in Propylene Glycol at Different Temperatures

Temp (°C)	τ (ns)	α_i	C_0 (M)	r_e (Å)	D (cm ² /s)	k_a (1/s)	χ^2_R
20	5.277	1.0000	0	(0.319)	1.86×10^{-7}	6.22×10^{13}	6.05
			0.500				
			1.000				
			1.500				
-20	8.519 4.953 0.277	0.317 0.464 -0.219	0	(0.317)	7.77×10^{-9}	5.28×10^{13}	3.59
			0.512				
			1.023				
			1.535				
-60	12.432 5.387	0.020 0.980	0	(0.318)	$<1 \times 10^{-15}>$	1.06×10^{13}	13.84
			0.524				
			1.048				
			1.572				

^aThe distance of the closest approach a was held constant at 5 Å during the analysis.

sitive to the precise value of r_e . In fact, r_e is poorly determined from the frequency-domain data alone, and use of the steady-state data is important in recovering the four variable parameters of the DDQ model (k_a , r_e , a , and D).

The reconstructed time-dependent decays computed using Eq. (6) and the parameters in Tables I and II from the best fits to the RBC and DDQ models are presented in Fig. 5. It is evident that the DDQ model predicts an initial rapidly decaying component, which occurs during the first 10 ps following excitation. The short-lived component in the intensity decay is responsible for the lower phase angles at higher frequencies. This rapid component in the decays is not provided by the RBC model (Fig. 5). The RBC model predicts no intensity decays of NATA quenched by acrylamide in the absence of diffusion at -60°C . Our ability to detect the short-lived component in the fluorescence intensity decay allowed us to detect the distance dependence of the quenching interaction. This distance dependence allows the DDQ model to account data for quenching even in vitrified propylene glycol in the absence of diffusion.

The fact that the DDQ model describes the quenching in the absence of diffusion indicates that the quenching interactions can operate through space without the fluorophore-quencher contact. This type of interaction in fluorescence quenching also explains the upward curvature of the Stern-Volmer plots. Finally, these results suggest that the distance-dependent quenching rate needs to be considered in the interpretation of acrylamide quenching of proteins containing tryptophanyl residues.

DISCUSSION

What types of quenching mechanism can account for a distance-dependent rate constant? It is known that both electron transfer and exchange (heavy atom) interactions depend exponentially on distance. We believe that our data are most consistent with an electron transfer mechanism. Electron ejection has been suggested to occur for indole [26,27]. Also, the rate constant near 10^{13} s^{-1} appears to be more consistent with electron transfer. In other studies using heavy atom quenchers, we have noticed that the k_a values were near 10^9 s^{-1} [28].

How does distance-dependent quenching affect the interpretation of data on dynamic quenching of proteins? In a pioneering study, Vanderkooi and co-workers [29] found that electron transfer in protein can occur over large distances, ranging to 15 Å. However, this long-range transfer was a consequence of the long lifetime of the phosphorescent state, so that even the $k(r)$ for electron transfer attenuated by these distances could decrease the phosphorescence decay time. Because of the short lifetime of the fluorescence state, electron transfer can occur over a more limited range of distances. However, because of the large value of $k(r)$, the rate constant for quenching can be comparable to the fluorescence lifetime for up to 4 Å beyond the contact distance of 5 Å. For instance, consider Eq. (1) with a r_e value of 0.32 Å and $k_a = 5 \times 10^{13} \text{ s}^{-1}$. At a distance of 4 Å the value of $k(r)$ is expected to be $0.19 \times 10^9 \text{ s}^{-1}$, or comparable to the decay rate of a fluorophore with a 5-ns lifetime, $\tau^{-1} = 0.2 \times 10^9 \text{ s}^{-1}$. Hence, some quenching of tryptophan

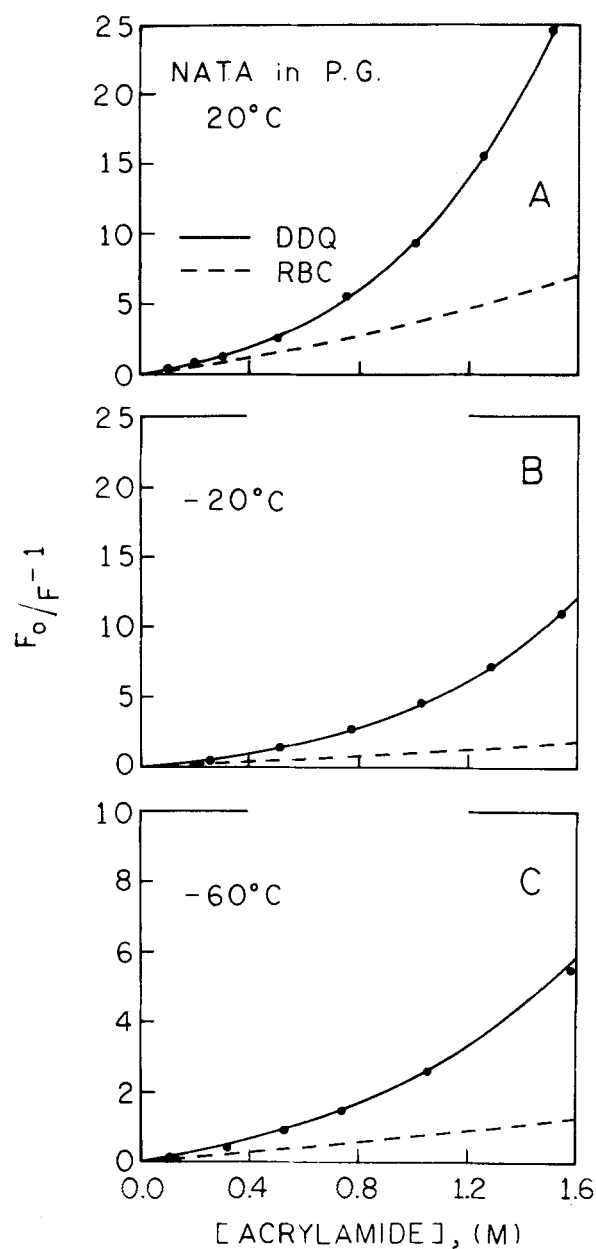


Fig. 4. Stern-Volmer plots for NATA in propylene glycol: (A) at $20^{\circ}C$; (B) at $-20^{\circ}C$, and (C) $-60^{\circ}C$ quenched by acrylamide (\bullet). The dashed lines represent the calculated values of $[(F_0/F) - 1]$ using the parameter values from the RBC model (Table I) and the solid lines represent the DDQ model (Table II). The RBC model predicts no quenching in the absence of diffusion (C).

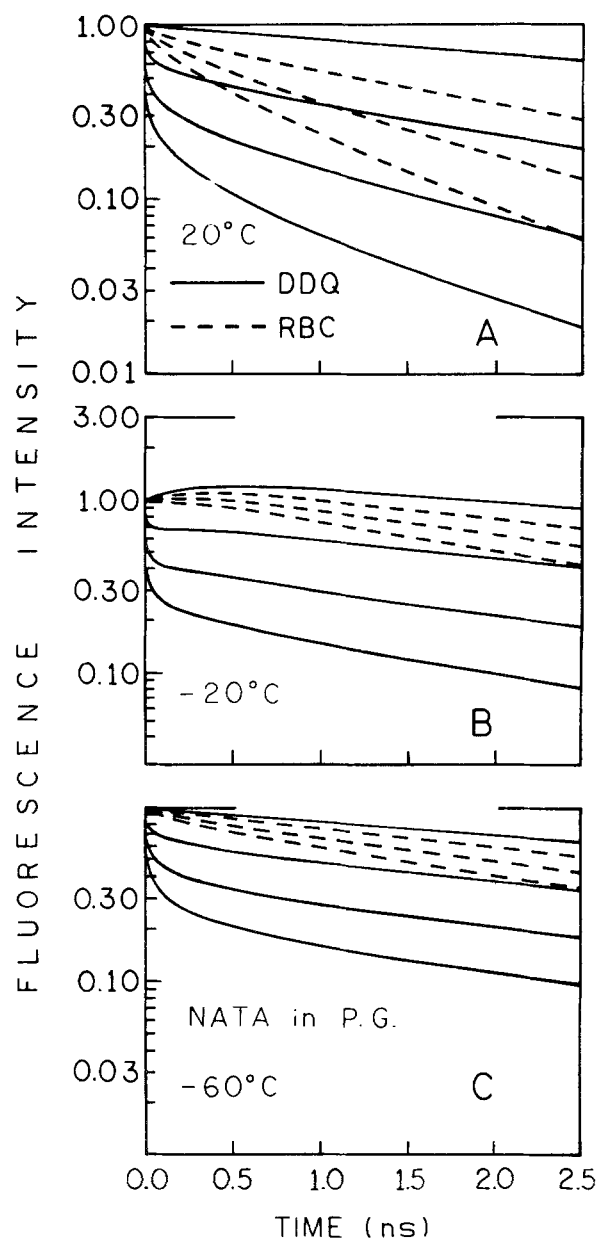


Fig. 5. Reconstructed time-dependent intensity decays of NATA in propylene glycol quenched by acrylamide: (A) 0, 0.5, 1.0, and 1.5 M at $20^{\circ}C$; (B) 0, 0.512, 1.023, and 1.535 M at $-20^{\circ}C$; and (C) 0, 0.524, 1.048, and 1.572 M at $-60^{\circ}C$, for the best fit RBC (---) and DDQ (—) parameters. The RBC model predicts no decays in the absence of diffusion (C).

tophan fluorescence may occur through space in proteins, but the quencher must still approach the fluorophore rather closely for quenching to occur. Hence, our results suggest that this effect should be considered in the inter-

pretation of protein quenching data but do not suggest a complete reinterpretation of this data. Of course one should also consider whether the polypeptide backbone provides an electron transfer quenching pathway.

ACKNOWLEDGMENTS

This work was supported by Grant GM-39617 from the National Institutes of Health, with support for instrumentation from NSF Grant DIR-8710401 and NIH Grant RR-07510.

REFERENCES

1. M. R. Eftink (1991) in J. R. Lakowicz (Ed.), *Topics in Fluorescence Spectroscopy, Vol. 2: Principles*, Plenum Press, New York, pp. 53–126.
2. M. R. Eftink and C. A. Ghiron (1981) *Anal. Biochem.* **114**, 199–227.
3. B. Somogyi and Z. Lakos (1993) *Photochem. Photobiol. B Biol.* **18**, 3–16.
4. J. R. Lakowicz and G. Weber (1973) *Biochemistry* **12**, 4171–4179.
5. J. R. Lakowicz, I. Gryczynski, H. Szmecinski, H. Cherek, and N. Joshi (1991) *Eur. Biophys. J.* **19**, 125–140.
6. J. R. Lakowicz (1982) in C. Ho *et al.* (Eds.), *Hemoglobin and Oxygen Binding, Vol. 1*, pp. 443–448.
7. C. D. Stubbs and B.W. Williams (1992) in J. R. Lakowicz (Ed.), *Topics in Fluorescence Spectroscopy, Vol. 3. Biochemical Applications*, Plenum Press, New York, pp. 231–271.
8. T. L. Nemzek and W. R. Ware (1975) *J. Chem. Phys.* **62**, 477–489.
9. J. C. Andre, M. Niclaude, and W. R. Ware (1978) *Chem. Phys.* **28**, 371–377.
10. J. R. Lakowicz, N. B. Joshi, M. L. Johnson, H. Szmecinski, and I. Gryczynski (1987) *J. Biol. Chem.* **262**, 10907–10910.
11. J. R. Lakowicz, M. L. Johnson, I. Gryczynski, N. Joshi, and G. Laczko (1987) *J. Phys. Chem.* **91**, 3277–3285.
12. I. Gryczynski, H. Szmecinski, G. Laczko, W. Wicz, M. L. Johnson, J. Kušba, and J. R. Lakowicz (1991) *J. Fluoresc.* **1**, 163–176.
13. J. R. Lakowicz and I. Gryczynski (1992) *Arab. J. Sci. Eng.* **17**, 261–286.
14. A. Szabo (1989) *J. Phys. Chem.* **93**, 6923–6939.
15. M. V. Smoluchowski (1917) *Z. Phys. Chem.* **92**, 129–168.
16. F. C. Collins and G. E. Kimball (1949) *J. Colloid Sci.* **4**, 425–437.
17. N. Joshi, M. L. Johnson, I. Gryczynski, and J. R. Lakowicz (1987) *Chem. Phys. Lett.* **135**, 200–207.
18. J. R. Lakowicz, J. Kušba, H. Szmecinski, M. L. Johnson, and I. Gryczynski (1993) *Chem. Phys. Lett.* **206**, 455–463.
19. J. R. Lakowicz, B. Zelent, J. Kušba, and I. Gryczynski (1994) in preparation.
20. N. J. Turro (Ed.) (1978) *Modern Molecular Photochemistry*, Benjamin Cummings, Menlo Park, CA, pp. 305–311.
21. J. R. Lakowicz, G. Laczko, and I. Gryczynski (1986) *Rev. Sci. Instrum.* **57**, 2499–2506.
22. G. Laczko, I. Gryczynski, Z. Gryczynski, W. Wicz, H. Malak, and J. R. Lakowicz (1990) *Rev. Sci. Instrum.* **61**, 2331–2337.
23. M. R. Eftink and C. A. Ghiron (1987) *Biochim. Biophys. Acta* **916**, 343–349.
24. C. A. Parker (1968) *Photoluminescence of Solutions*, Elsevier, New York, pp. 220–226.
25. J. R. Lakowicz, B. Zelent, J. Kušba, I. Gryczynski, and M. L. Johnson (1994) *Photochem. Photobiol.* (submitted).
26. E. P. Kirby and R. F. Steiner (1970) *J. Phys. Chem.* **74**, 4480–4490.
27. R. F. Steiner and E. P. Kirby (1969) *J. Phys. Chem.* **73**, 4130–4135.
28. J. R. Lakowicz, B. Zelent, J. Kušba, and M. L. Johnson (1994) *J. Phys. Chem.* (in preparation).
29. J. M. Vanderkooi, S. W. Englander, S. Papp, W. W. Wright, and C. S. Owen (1990) *Proc. Natl. Acad. Sci. U.S.A.* **87**, 5099–5103.